ORIGINAL RESEARCH ARTICLE

Effect of Citrate-Based Bath pH on Properties of Electrodeposited Cu–Zn Coating on an Aluminum Substrate

RASİM ÖZDEMİR, ERSİN ÜNAL, and İSMAİL HAKKI KARAHAN

In this study, Cu–Zn alloys were deposited in citrate-based electrolytes on aluminum substrate by electrodeposition method. The effect of bath pH variation on the properties of the obtained Cu–Zn alloy coatings was investigated. The electrochemical behavior of the citrate-based baths and the crystalline structure, surface morphology and elemental content, electrical resistivity and thermal behavior of the alloy coatings were analyzed. According to the results of cyclic voltammetry (CV) analysis, increasing bath pH caused a negative shift in the cathodic deposition potential. In addition, the anodic dissolution peaks first shifted to the positive side with increasing pH and then shifted back to the negative direction. According to the results of XRD analysis, the phase structure of Cu–Zn alloys generally consists of α and β' phases, but according to differential scanning calorimeter (DSC) analysis, it is possible that there is a γ phase in the structure in addition to these phases. In addition, pH increase (4.5 to 6.5) caused a relative increase in crystal grain size (~14 to ~ 25 nm). The Zn content of Cu–Zn coatings first increased (~pct 15 to ~ pct 55) with pH increase, then followed a horizontal trend (~pct 55 to ~ pct 59) with further pH increase and then exhibited a slight decreasing trend (~pct 59 to ~ pct 52). The pH increase significantly affected the surface morphology of the coatings and denser coatings were obtained with increasing pH. While the electrical resistivity of Cu–Zn coatings first increased (0.0408 to 0.0696 $\mu\Omega$cm for 297 K) with increasing pH, it tended to decrease (0.0696 to 0.0479 $\mu\Omega$cm for 297 K) again at higher pH values. In addition, the electrical resistivity of the coatings increased with increasing measurement temperature. According to DSC analysis of the coatings, endothermic peaks were obtained, possibly representing the transformation from γ to β' phase.

RASİM ÖZDEMİR is with the Vocational School of Technical Science, Kilis 7 Aralık University, 79000 Kilis, Turkey. ERSİN ÜNAL is with the Department of Mechanical Engineering, Faculty of Engineering and Natural Sciences, Osmaniye Korkut Ata University, 80000 Osmaniye, Turkey. Contact e-mail: ersinunal@osmaniye.edu.tr İSMAİL HAKKI KARAHAN is with the Department of Physics, Faculty of Arts and Sciences, Mustafa Kemal University, 31040 Hatay, Turkey.

Manuscript submitted March 25, 2024; accepted July 13, 2024.
Article published online July 26, 2024

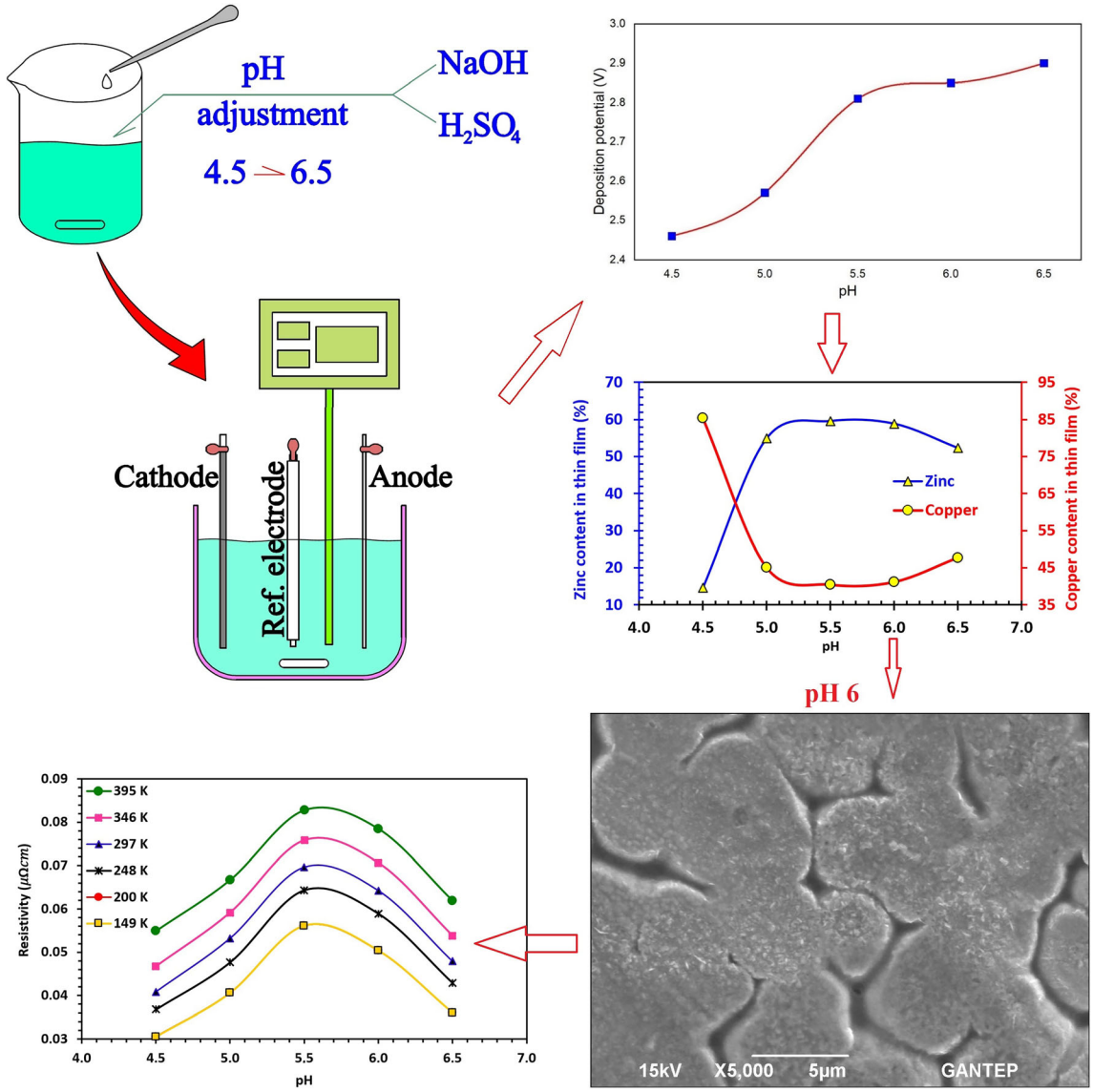

https://doi.org/10.1007/s11661-024-07524-3

I. INTRODUCTION

THE outermost layer of a material is its surface, and since material interactions with the environment take place on the surface, it has an important place in the durability and efficiency of engineering components. Therefore, improving the properties of its surface is an effective and preferred method to improve the performance of industrial components.[1] One of the most effective ways to improve the surface of materials is to coat the outer surface with a suitable material.[2] There are many methods for producing metal and alloy coatings and among them electrochemical deposition technique is one of the most widely used methods due to its wide range of advantages. The electrodeposition process is a unique technique that uses an electric field to deposit metal or alloy coatings on conductive substrate in an electrolyte. Coatings produced by electrodeposition are uniform, strong, and economical compared to other manufacturing processes.[3,4] This method has significant advantages such as simplicity and ease of use and allows for effective control of production parameters. Compared to pure metal coatings, electrochemically deposited alloys show better properties as their chemical composition can be changed according to the desired function. Since the various properties of alloys

are significantly influenced by both their composition and structure, reliable control of the composition and structure of these engineering alloys is an important factor for their wide application in industry. The properties of an electrodeposited film are influenced by many parameters such as current density, bath pH, deposition potential, and electrolyte composition and amounts.[5–9] It is obvious that a large number of experimental studies are required to find the best values for different combinations of these electroplating parameters in order to obtain effective and applicable alloy coatings.

As an important engineering material, aluminum and its alloys are widely used in various industries such as aerospace, automotive, household, defense, electronics, and air conditioning due to their significant advantages such as affordable cost, recyclability, excellent thermal and electrical conductivity, low density, low specific gravity, and high specific strength. However, in some special and challenging cases, aluminum and its alloys may need to be supported by coatings with various properties to expand their industrial applications. Surface modifications of aluminum and its alloys can offer a wide range of electrical, chemical, mechanical, and decorative properties.[10–14] Today, copper, zinc, and their alloys find applications in a wide variety of industrial fields, both in bulk and as coatings. Cu–Zn alloys have a wide range of industrial applications depending on their elemental content and the heat and mechanical treatments applied. For this reason, it is probably considered one of the most important alloys after steel in engineering applications. In addition to corrosion protection, they are also used in magnetic, decorative, and electrical applications. Cu–Zn alloys, also called brass, are still of great interest to researchers due to their low cost, environmental compatibility, mechanical durability, high hardness compared to pure metal coatings, and beautiful color (golden yellow). These properties make Cu–Zn alloys an indispensable material in many critical areas such as the manufacture of precision instruments, electronic products, and batteries. For example, Cu–Zn alloys are widely used as electrical contact materials in microelectronic devices, automotive connectors, electrical machinery, and electronic instruments. The materials used in the electrical contact application are usually Cu–Zn alloys, which are of interest for their excellent electrical conductivity and low material cost.[15–19] Another important feature of the Cu–Zn alloy system is its shape memory capability, which occurs when the material changes shape by heating due to phase transformation (martensite to austenite). Shape memory materials are characterized by their ability to change shape by heating or cooling under certain conditions and to make countless cycles between different shapes. This important property allows Cu–Zn materials to be used in critical application areas such as actuators, sensors, micro-sized materials, and micro-electromechanical systems.[3,20–24]

On a commercial scale, brass plating is a plating process produced by zinc and copper deposition followed by a thermal diffusion step. Direct electroplating can be challenging due to the more than 1 V difference between the reduction potentials of zinc and copper, and for a successful co-deposition bath, complexing agents such as cyanide are added to the electrolyte to reduce the difference between the reduction potential values. However, there is a need for satisfactory alternative electrolytes due to many concerns about the biological toxicity and environmental damage of cyanide-based baths. Among the alternative electrolytes suggested in the literature, citrate baths seem more likely. Citrates, which are non-toxic, have low molecular mass, and can form stable complexes with a variety of metals, cause waste that is easier to deal with.[25] Citrates are a strong complexing agent for many metals such as copper, nickel, zinc, iron, tungsten, and cobalt making them one of the most commonly used additives in electroplating. Citrates can also improve deposition efficiency by inhibiting the hydrogen formation reaction, which partially blocks the electrode surface.[26] Citrate electrolytes can be used for electrodeposition with good quality, low cost, and high current efficiency. Citrates can also act as buffering, polishing, and leveling agents, thus eliminating the need for other electrolyte additives.[27] Dridi *et al.*[25] studied the effect of different Cu/Citrate concentrations and bath pH on the electrochemical deposition mechanism of Cu–Zn alloys and stated that the bath pH value is a significantly effective parameter on the Cu-citrate species in the electrolyte. The authors stated that the citrate species formed at pH values higher than 5 played a relatively inhibitory role in Cu deposition, while the citrate species formed at pH values lower than 5 supported Cu reduction. In another study, Karahan[28] investigated the effect of pH on the electrodeposition of Zn–Co alloys and stated that the pH value of the bath is closely related to the homogeneity and density of the coating. The author also stated that pH value is a parameter that directly affects the corrosion resistance of Zn–Co coating. Dulal *et al.*[29] investigated the effect of bath pH (3 to 8) on the electrodeposition of Co–W–P ternary alloy and reported that the pH change greatly affected the elemental content of the alloy films obtained. The authors stated that the content of Co, the main element of the alloy, in the coating increased from 48 to 70 pct when the pH value increased from 3 to 5 and followed a horizontal course until pH 7. At higher pH values, they stated that the Co content started to decrease. Kazimierczak ve Ozga,[30] in their study on Sn-Zn alloy in citrate-based baths, stated that electrolytes with pH 6.5 and above are unstable, while electrolytes in the pH 1-4 range have low tin solubility. For these reasons, the authors recommended a pH value of 5. Green *et al.*[27] reported in their study on the deposition of Cu–Ni alloys in citrate electrolytes that citrate electrolytes at pH 4 were unstable. The authors stated that the electrolyte with pH 6 was stable for several weeks and that Cu–Ni alloy electrodeposition with high current efficiency could be performed in these electrolytes. Kazimierczak *et al.*[31] used citrate-based baths for electrodeposition of Zn–Mo alloys. The authors reported that the Mo content in the alloy decreased with increasing citrate bath concentration and a maximum Mo content of around 50 pct was obtained. The authors also stated that the optimal conditions for the electrodeposition of

Zn–Mo alloys from citrate baths are in a narrow pH range between 4 and 6. Kahoul *et al*.,[26] in their study on the deposition of Zn–Co alloys in citrate-based baths, reported that they obtained Co content around 15 pct at pH 5.6. According to the CV results, the authors stated that increasing bath pH caused a decrease in cathodic current density, and the deposition potential also shifted to negative values with increasing pH.

It is possible to say that the studies on the deposition of Cu–Zn alloys in citrate-based baths are not yet sufficient level. First of all, pH is a very effective and important production parameter for electrodeposition and complexing additives used in this process. In addition, in citrate-based baths, the pH effect on the activity of metal/citrate species is extremely high. There are a few studies in the literature on the variation of pH values of the electrolytes used in the deposition of citrate-based Cu–Zn alloys. However, it is seen that these studies focused on electrodeposition mechanisms. We have not come across any studies on the effect of electrolyte pH variation on the properties of the final product Cu–Zn coatings. In this study, for the first time in the literature to the best of our knowledge, the effect of the electrolyte pH value on the properties such as crystal structure, surface morphology, elemental content, electrical resistivity of the thin films produced by keeping the citrate bath concentration constant in the deposition of Cu–Zn alloys was investigated and thermal analysis of the coatings was also performed.

II. EXPERIMENTAL DETAILS

Cu–Zn alloys were produced by electrochemical plating method on aluminum substrate in electrolytes adjusted to different pH values. The bath content consisted of $CuSO_4{\cdot}5H_2O$ (0.6 M/lt), $ZnSO_4{\cdot}7H_2O$ (0.2 M/lt) and sodium citrate ($Na_3C_6H_5O_7$, 0.5 M/lt) as complexing agent. All chemicals are of high purity and were obtained from Merck company. The pure aluminum substrates were first sanded (grades 1000-1800-2400) for polishing and remove various undesirable substances such as dirt, oil, and oxide layer on the surface. The substrate was then activated in 1 M sodium hydroxide (NaOH) solution with surfactant heated to 70 °C for 5 seconds, rinsed in double distilled water, and allowed to dry in the open air. The substrate surface for deposition was set to 3.8 cm^2. A three electrode deposition system was used to produce Cu–Zn coatings. An aluminum substrate was used as the cathode, a platinum rod as the anode, and a saturated calomel electrode (SCE) as the reference electrode. The electrodeposition process was carried out in a conventional glass cell in a non-ventilated environment. The current density was set to 8 mA/cm^2 and the deposition time was 60 minutes. The bath temperature is 24 °C and stirred at 400 rpm during deposition. The electrolyte was prepared using double distilled purified water and all chemicals used were of high purity. Bath pH values were adjusted using NaOH or sulfuric acid (H_2SO_4). The bath parameters and electrolyte components are schematically shown in Figure 1.

CV curves were recorded in the range of + 0.5 V to − 1.6 V and at a scan rate of 10 mV/s. CV curves were obtained in a freshly prepared bath using a Parstat 2273 electrochemical instrument. X-ray patterns (XRD) were obtained with a Rigaku diffraction device to examine the crystal structures of the coatings. XRD was performed at 30 mA and 30 kV, with a 2θ range of 20 to 90 deg using CuKα radiation at a rate of 0.05 deg, 2θ/0.5 seconds. The crystal grain size (D) of the samples was calculated by the Debye–Scherrer Eq. [1] given below. Micro strain values were calculated by the following Eq. [2].[32,33]

$$D = \frac{0.9x\lambda}{\beta x\cos\theta} \quad [1]$$

$$\varepsilon = \frac{\beta x\cos\theta}{4} \quad [2]$$

In Eqs. [1] and [2], β is the width at half height in radians (FWHM) of the corresponding XRD peak, θ is the Bragg reflex angle of the peak, and λ is the wavelength of the X-ray used. Grain size and microstrain values were also calculated using the Williamson–Hall (W–H) method. According to Williamson and Hall, the broadening of the diffraction line is due to the contribution of crystallite size (β_D) and strain (β_ε).

$$\beta_T = \beta_D + \beta_\varepsilon \quad [3]$$

$$\beta_T = \frac{K\lambda}{D\cos\theta} + \varepsilon 4\tan\theta \quad [4]$$

If Eq. [4] is rearranged,

$$\beta_T\cos\theta = \varepsilon 4\sin\theta + \frac{K\lambda}{D} \quad [5]$$

In Eq. [5], the values of $\beta_T\cos\theta$ on the y-axis are plotted as a function of $4\sin\theta$ on the x-axis and linear fitting is performed. With the linear fitting process, a line equation is obtained in the form $y = m{\cdot}x + c$. While the microstrain value is obtained by using the slope ($m = \varepsilon$) of this line drawn by the W–H method, the crystallite size is calculated from the y-intercept value $\left(c = \frac{K\lambda}{D}\right)$.[34–36]

The following equations were used to calculate the relative texture coefficient ($RTC_{(hkl)}$) values of Cu–Zn alloy coatings.[37–39]

$$RTC_{(hkl)} = 100 \times \frac{TC_{(hkl)}}{\sum TC_{(hkl)}} \quad [6]$$

$$TC_{(hkl)} = \frac{I_{(hkl)}}{\sum I_{(hkl)}} \times \frac{\sum I_{0(hkl)}}{I_{0(hkl)}} \quad [7]$$

In Eq. [6], $TC_{(hkl)}$ is the texture coefficient of the corresponding (hkl) plane and $\sum TC_{(hkl)}$ is the sum of

the texture coefficients of all planes in the XRD pattern. In Eq. [7], $I_{(hkl)}$ is the intensity value of corresponding peak and $\sum I_{(hkl)}$ is the sum of the intensities of all peaks in the pattern. $I_{0(hkl)}$ and $\sum I_{0(hkl)}$ are the intensity of the corresponding peak and the sum of the intensities of all peaks in the pattern, respectively, obtained from the reference card. XRD pattern data of the β phase of Cu_1Zn_1 alloy with reference code 98-062-9462 were used for RTC calculations.

The surface structure of Cu–Zn coatings was investigated by scanning electron microscopy (SEM). The chemical composition of Cu–Zn coatings was determined by energy-dispersive X-ray spectrometry (EDS) analysis. Measurements were taken from three different regions of each sample to verify that the results were compatible with each other. JEOL JSM-5500LV (Japan) brand and model device was used for SEM and EDS analysis. Differential Scanning Calorimetry (DSC) measurements were performed with a Perkin Elmer brand, Pyris-6 model DSC device in the range of 0 °C to 400 °C. Measurements were made in vacuum environment.

Four-point probe method was used for resistance measurements of Cu–Zn coatings. For the measurement, electrodes were attached to the contact points with silver paint. The thermal stress effect was eliminated by averaging the voltage values obtained with current in both directions at each temperature. The ohmic behavior of the contacts in the studied temperature region was verified by linear variations of the I–V characteristics, which are independent of changing the direction of the applied currents. To ensure that the resistance values obtained from the samples are reliable, each sample was measured several times. The samples were placed on the cold finger of a Janis liquid nitrogen cryostat and the temperature was accurately monitored with a Lake-Shore 320 temperature controller. Temperature-dependent conductivity measurements (in the temperature range 100 K to 350 K) were made with a Keithley 2400 source measurement unit.

III. RESULTS AND DISCUSSION

The baths were adjusted to different pH electrolyte values and Cu–Zn alloy thin films were deposited at current density values of 16 and 8 mA/cm^2. Most of the thin films produced at 16 mA/cm^2 were found to have excessive brittleness and a problem of adhesion to the substrate, which is an obstacle for resistivity measurement. Therefore, Cu–Zn deposition was carried out at 8 mA/cm^2. The amounts of $CuSO_4$, $ZnSO_4$, and sodium citrate in the electrolyte were kept constant and the pH value was changed between 3.5 and 8 to produce thin films on aluminum substrates. In the studies, it was observed that thin films were not formed at pH 3.5 and 4. Thin films were formed at pH values of 7, 7.5, and 8, but extremely brittle films were obtained. Moreover, due to the adhesion problem of these films on aluminum substrates, spills occurred during production. Therefore, Cu–Zn thin films were deposited at bath pH values of 4.5, 5.0, 5.5, 6.0, and 6.5. Szczygiel and Laszczynska[40] investigated the effect of pH on the electrodeposition of Zn–Ni–Mo alloy in a citrate bath. The authors reported that the thickness of the films produced at pH 7.5 was much thinner (from 10.4 to 0.8 μm) compared to the films produced at pH 5.7 and 4.5 due to very low current efficiency and intense crack formation was observed in the coatings due to large internal stress.

A. *Deposition Bath, Potential, and CV Analysis*

Figure 2 shows the appearance of citrate-based Cu–Zn deposition baths at pH 4.5 and pH 6.5. The natural pH value of the prepared untreated bath is measured as 4.66. As can be seen from the figure, the color of the bath is a different shade of blue and it is noticed that the color of the bath starts to darken with the increase in pH. The pH change has an effect on the metal citrate species in the bath and different pH values lead to the formation of different citrate species. This also changes the activity of Cu and Zn ions.[25] Probably these changes in the bath cause the color of the bath to change. Another important point is that the bath can remain stable for a long time in terms of industrial use. It is possible to say that the baths obtained are extremely stable even though they are kept for more than a month. During this period, no precipitation *etc*. was observed in the baths. Moreover, Cu–Zn deposition process could be carried out without any problems in these aged baths.

It is useful to consider the chemical reactions related to the deposition of Cu and Zn metals in citrate baths separately. Because different types of citrate are effective for Cu and Zn metals under different conditions. The formation of copper-citrate complexes is represented by the following general reaction equation.[25,41]

$$pCu^{2+} + qCit^{3-} + rH^{+} \leftrightarrow Cu_pCit_qH_r^{(2p-3q+r)^{+}} \quad [8]$$

At pH values greater than 4, the $(Cu_2Cit_2H_{-1})^{3-}$ and $(Cu_2Cit_2H_{-2})^{4-}$ copper-citrate species become active and the chemical reactions according to these species are as follows. As the pH value increases after 4, the effect of the $(Cu_2Cit_2H_{-1})^{3-}$ species decreases and the effect of the $(Cu_2Cit_2H_{-2})^{4-}$ species increases.[25,41]

$$2Cu^{2+} + 2Cit^{3-} = Cu_2Cit_2H_{-1}^{3-} + H^{+} \quad [9]$$

$$2Cu^{2+} + 2Cit^{3-} = Cu_2Cit_2H_{-2}^{4-} + 2H^{+} \quad [10]$$

For example, in reaction (10), the discharge of $Cu_2Cit_2H_{-2}^{4-}$ species occurs in two stages as follows.[42]

$$Cu_2Cit_2H_{-2}^{4-} + 2e^{-} = Cu_2Cit_2H_{-2(ads)}^{6-} \quad [11]$$

$$Cu_2Cit_2H_{-2(ads)}^{6-} + 2e^{-} + 2H_2O = 2Cu + 2Cit^{3-} + OH^{-} \quad [12]$$

In terms of zinc-citrate complexes, $Zn(HCit)^{-}$, $(ZnH_2Cit_2)^{4-}$, and $(ZnH_2Cit)^{0}$ species are active after

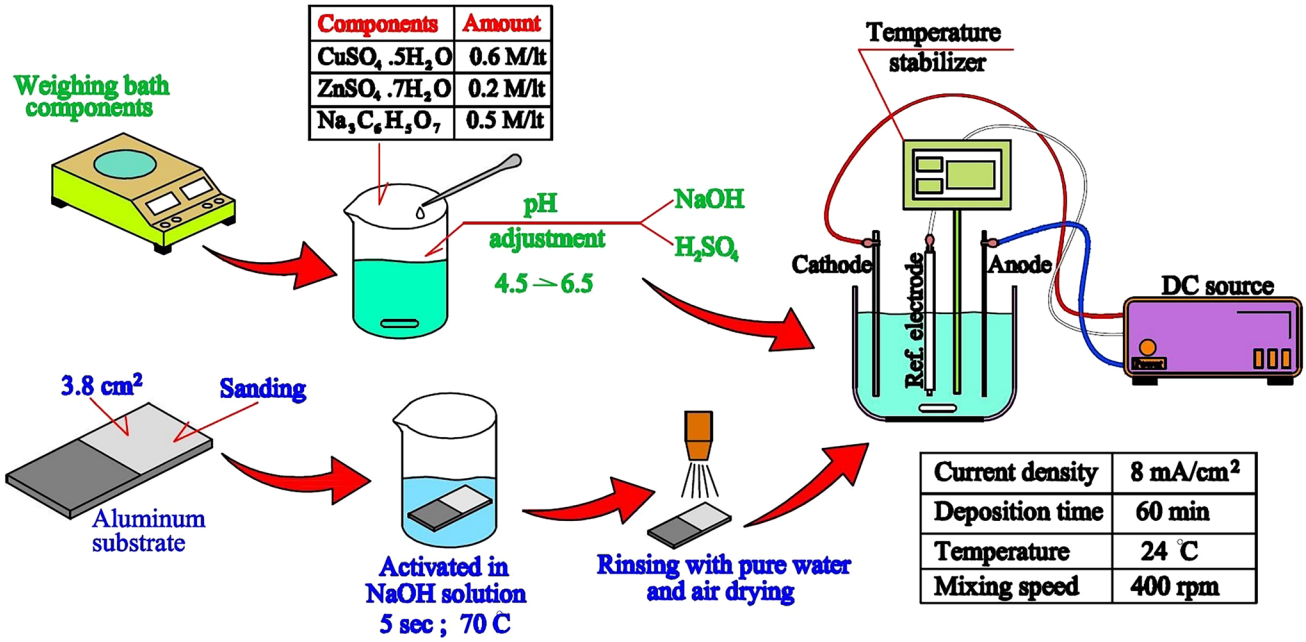

Fig. 1—Production process, bath components, and production parameters of Cu–Zn coatings.

pH 4. However, since $(ZnH_2Cit_2)^{4-}$ species is not electroactive, Zn deposition is probably realized through the other two types of Zn-citrate complexes. The electrode reactions related to Zn deposition are as follows.[43]

$$Zn(HCit)^- + H_2O + 2e^- = Zn^0 + H_2Cit^{2-} + OH^- \quad [13]$$

$$(ZnH_2Cit)^0 + 2e^- = Zn^0 + H_2Cit^{2-} \quad [14]$$

In addition, hydrogen evolution reactions can also take place in citrate-based baths. The reactions that can take place are given below. Of the following reactions, reaction (18) is expected to occur only at high potentials.[43]

$$H_4Cit^0 + 2e^- = H_2 + 2H_2Cit^{2-} \quad [15]$$

$$H_3Cit^- + 2e^- = H_2 + HCit^{3-} \quad [16]$$

$$2H_2Cit^{2-} + 2e^- = H_2 + 2HCit^{3-} \quad [17]$$

$$2H_2O + 2e^- = H_2 + 2OH^- \quad [18]$$

The behavior of the baths in which Cu–Zn alloys were electrodeposited at different pH values was investigated on CV curves and is given in Figure 3. From Figure 3, it is seen that the Cu–Zn bath with a pH value of 4.5 proceeds around zero current density in a very short voltage range after a broad peak corresponding to possible outgassing in the range of + 0.5 V to − 0.7 V at the beginning of the cathodic scanning direction. Then, around − 0.9 V, the current density started to increase due to the reduction reactions accompanied by H_2 outgassing as well as Cu–Zn alloy deposition and the current density increase accelerated especially after − 1.3 V. When the anodic scanning direction is examined, two different dissolution peaks of the Cu–Zn alloy around − 0.65 V (peak A) and just after 0 V (peak B) stand out. These peaks correspond to the dissolution of the different phases of the Cu–Zn alloy formed during scanning in the cathodic direction.[44] Moving further in the anodic scanning direction, a current increase is observed after + 0.2 V, again indicating possible outgassing. A similar situation is noticed in the CV curves of Ni–B alloy coatings made by Ünal *et al.*[2] and recorded at pH 4, and current increases are observed both at the beginning of the anodic direction and at the end of the cathodic direction. It can be stated that these current increases tend to occur around pH 4. When the CV curves obtained in Cu–Zn alloy electrolytes with pH 5 and higher are examined, it is understood that the current increases indicating possible outgassing seen in the bath with pH 4.5 are not observed. In the bath with a pH value of 5, it is noticed that the current value proceeds at zero level until − 1.0 V in the cathodic scanning direction. After this value, current increase started and accelerated after − 1.3 V. In this bath, the current increase, which started around − 0.7 V representing dissolution in the anodic direction, decreased to zero level by forming a peak (B) around + 0.15 V. In the bath with a pH value of 5.5, it is seen that the potential to start deposition in the cathodic scanning direction shifted to the negative side and started around − 1.25 V. In the anodic scanning direction, although a slight increase in current passage was observed up to around 0 V, a clear dissolution peak appeared only around 0.1 V (B). In the CV curve of the bath with pH

6, the deposition potential in the cathodic direction also started around − 1.25 V, but the rate of current increase was higher compared to pH 5.5. In the anodic direction of the pH 6 bath, a broad and flattened dissolution peak is observed around − 0.4 V (A), as well as a sharper dissolution peak around + 0.05 V (B). It can be stated that the CV curve of the bath at pH 6.5 is similar to pH 6. In general, it appears that increasing pH shifts the potential of the Cu–Zn alloy to start deposition to the negative side. In fact, the coating contents in terms of pH variation also support this conclusion (see Table I and Figure 5), the Zn content in the coating increased with increasing pH up to pH 5.5 and showed a slight decrease at higher pH values. Since the deposition potential of Zn metal alone (− 1.2 V) is on the more negative side compared to Cu metal, a negative shift in the deposition potential seems to be quite normal. Moreover, since there was no significant change in Zn content after pH 5.5, the deposition potential did not shift more negatively. An increase in the pH of the bath leads to a decrease in the amount of H^+ (protons) in the electrolyte, which in turn leads to a decrease in the hydrogen evolution reaction accompanying the deposition of Cu–Zn metal.[29,45,46] Despite this, the increase in the deposition potential supports our theory about the Zn content. It can be said that the CV curves obtained are consistent with the CV curves of Cu–Zn alloys in the literature.[15] When the CV curves were evaluated in terms of pH change, the rate of current increase in the cathodic direction increased up to pH 5.5 and decreased again at higher values. A similar trend is observed in the dissolution peaks in the anodic scanning direction (B) in the CV curves. With increasing pH, the height of the peaks first increased (up to pH 5.5) and then started to decrease. In addition, the dissolution peaks first shifted to the positive side with increasing pH and then shifted back to the negative direction. This can also be related to the Cu and Zn content values in the coating (see Table I and Figure 5). The Zn content increased up to pH 5.5 and tended to decrease at higher pH values. It is possible to express the opposite situation for Cu content. A dissolution peak occurred only at pH 4.5 and 5, and no A dissolution peak was observed at higher pH values. In addition, crossover between forward and backward scanning in CV curves characterizes the formation of new phases.[15] These crossovers are defined as indicators of nuclei formation and are caused by the voltage difference between the deposition and dissolution processes.[47,48] Shin *et al.*[49] investigated the effect of citrate complexing agent and pH on Cu and Zn electrodeposition. The authors reported that the presence of citrate complexing agent in the electrolyte, especially at pH 4.7, reduced the difference between Cu (− 0.2 V to − 0.5 V) and Zn (− 1.2 V to − 0.7 V) deposition potentials and thus facilitated the deposition of these two metals together as alloys. Winiarski *et al.*[50] reported that in the electrodeposition of Zn–Fe–Mo alloys, the cathodic deposition potential shifted to more negative sides and the cathodic current density decreased with the effect of increasing bath pH. The authors stated that if the oxide formation rate on the cathode surface exceeds the reduction rate at a later stage, the cathode surface may be blocked and these changes in the cathodic direction may be due to this. Kazimierczak ve Ozga[30] in their study on Sn–Zn alloy in citrate-based baths investigated the effect of different pH values on hydrogen formation in citrate-only electrolytes. The authors reported that hydrogen evolution at pH 2–6 is the result of reduction of protonated forms of citrate ions, while at higher pH values (6–9), it is the result of water dissociation.

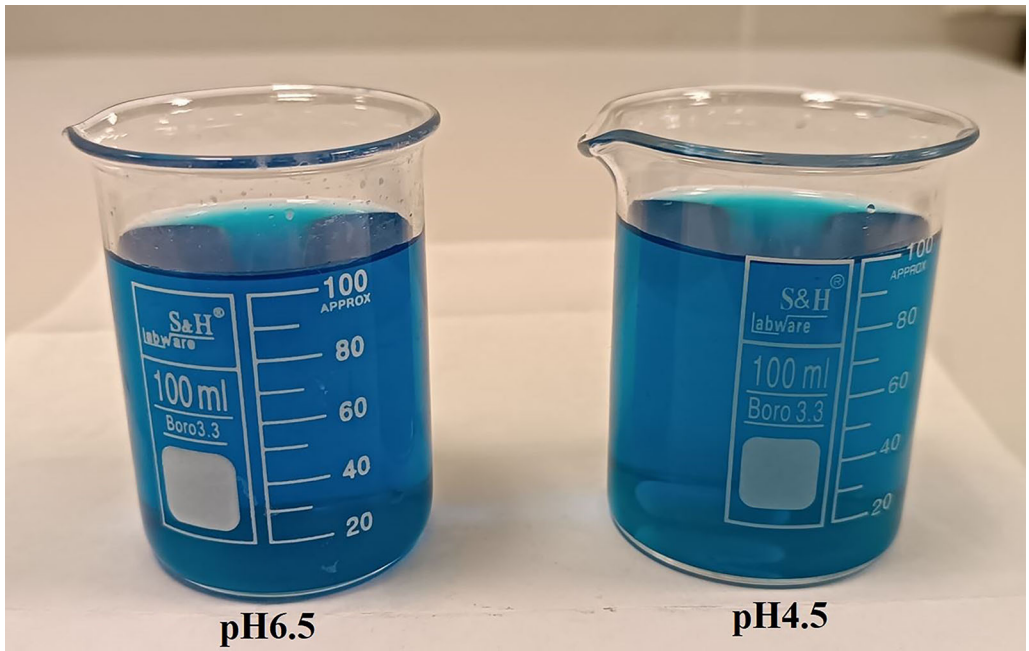

Fig. 2—Appearance of Cu–Zn electrodeposition baths at different pH values.

Figure 4 shows the effect of electrolyte pH on the average deposition potentials of Cu–Zn coatings deposited at a constant current value of 8 mA/cm^2. It is seen that the deposition potentials of Cu–Zn films vary between 2.4 and 2.9 V. It was revealed that with the increase in electrolyte pH value, there is an increase in the deposition potential in order to keep the constant current value in equilibrium. Especially up to pH 5.5, the deposition potential increased rapidly, but after pH 5.5, the potential continued to increase but followed a more horizontal course. In addition to the decreasing H+ ions with increasing pH value, the nature of the electrolyte changes with the effect of increasing OH− ions, which is reflected in the storage potential. The increase in Zn deposition rate up to pH 5.5 seems to contribute to the faster increase in the deposition potential. At values above pH 5.5, a slight decrease in Zn content slows down the increase in deposition potential. Winiarski *et al.*[50] investigated the effect of pH increase on the deposition potential of Zn–Fe–Mo alloy coatings at constant current (20 mA/cm^2). According to the authors, pH increase caused an increase in the deposition potential (from around − 1.13 V to around − 1.32 V). The authors stated that this increase may be due to the blockage of the cathode surface by metal oxides or hydroxides resulting from the strong alkalization of the electrolyte near the cathode surface.

B. *XRD Analysis*

XRD patterns were obtained to evaluate the effect of electrolyte pH on the crystal structures of electrodeposited Cu–Zn coatings and are presented in Figures 4 and 5. Figure 6 shows the graphs drawn by Williamson–Hall (W–H) method according to the information obtained from XRD patterns. The parameters calculated from the XRD patterns and the contents of the coatings for easier comparison are given in Table I. In addition, grain size and microstrain values calculated from the graphs obtained by W–H method are also given in Table I. In the XRD patterns shown in Figure 5, it is understood that the (111) and (110) peaks specific to Cu–Zn alloys are around 43 deg, the (200) peak is around 63 deg, and the (200) peak is around 79 deg. Apart from these peaks, only the (220) peak around 75 deg in the sample with a pH value of 4.5 is reflected in the XRD pattern, albeit weakly. The sample with a pH value of 4.5 has a face-centered cubic (FCC) structure and is in α phase.[17,51,52] According to the equilibrium diagram of Cu–Zn alloys, the α phase is formed when the zinc content is less than 30 pct and the Zn content given in Table I supports this situation.[53–55] Li *et al.*,[56] in their study on Cu–Zn alloy plating, similarly obtained the (111) peak around 43 deg and stated that this peak belongs to $Cu_{0.7}Zn_{0.3}$ alloy indexed to reference pdf card 03-065-9062. They reported that the presence of this peak indicates the co-deposition of Cu–Zn atoms and the formation of substitution solid solution due to Cu and Zn elements with similar diameter and atomic number. It is understood that the samples produced at other pH values (5, 5.5, 6, 6.5) have body-centered cubic (BCC) structure and β' phase. According to the Cu–Zn equilibrium diagram, when the Zn content is around 50 pct, the β' phase is formed and with the increase in zinc content, this phase can be accompanied by the γ phase.[53–55,57] The Cu–Zn alloy deposits we obtained are in general agreement with the diffraction peaks in the XRD pattern of the β' phase (Cu_1Zn_1) with reference

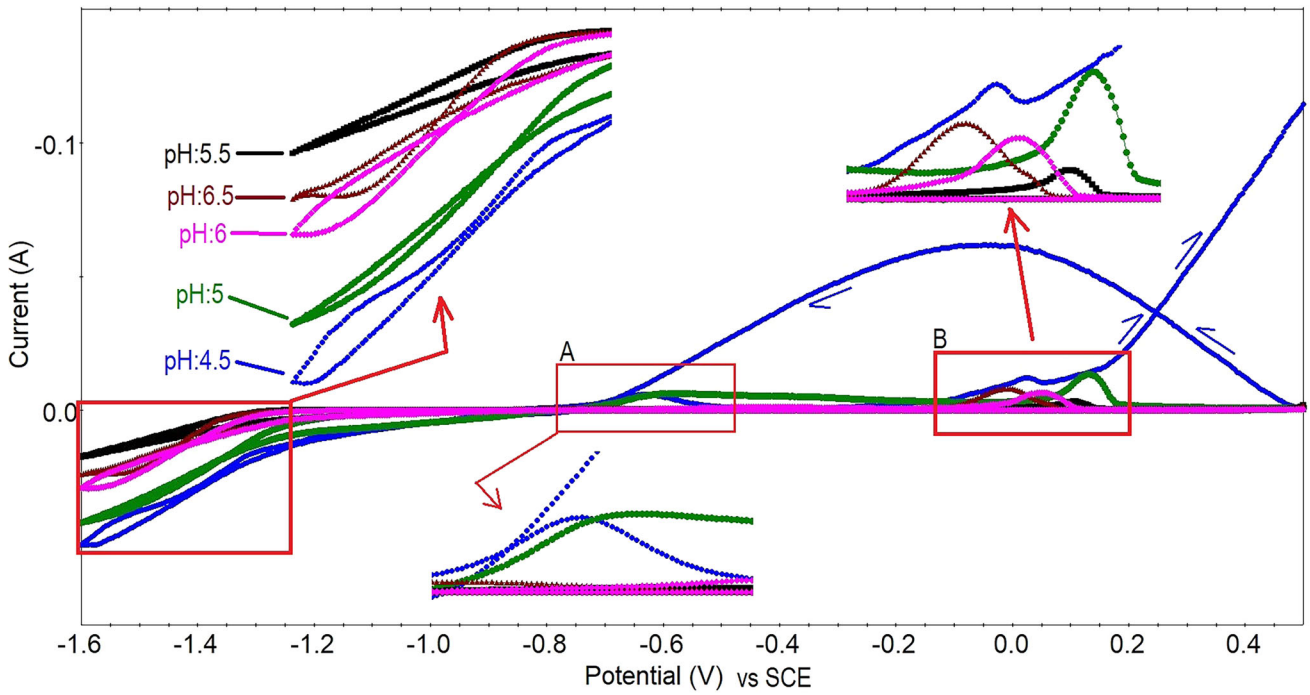

Fig. 3—CV curves of Cu–Zn coatings obtained from electrolytes adjusted to different pH values.

Table I. Parameters Obtained from XRD Patterns of Cu–Zn Thin Films Produced by Varying the pH Ratio

Electrolyte pH Value	Cu pct Content in the Film	Zn pct Content in the Film	2θ (degree)	d (A°)	FWHM (degree)	(hkl)	Latis (a) (nm)	Grain Size from Debye-Scherrer, nm (Belongs to the Highest Peak)	Average Grain Size from Debye–Scherrer, nm	Grain Size Calculated from W–H Plot	Microstrain from Eq. [2] (Belongs to the Highest Peak), x10^{-3}	Average Microstrain from Eq. [2], $\times 10^{-3}$	Microstrain Calculated from W–H Plot, $\times 10^{-3}$
4.5	85.39	14.60	43.24	2.0904	0.595	111	0.370	14.3	63.3	6.1	6.55	3.52	8.83
5.0	45.04	54.95	43.24	2.0903	0.359	110	0.303	23.8	22.8	25.3	3.95	3.12	0.298
5.5	40.39	59.60	43.34	2.0858	0.624	110	0.348	13.7	20.7	8.1	6.85	4.4	4.74
6.0	41.11	58.88	43.25	2.0901	0.397	110	0.305	21.5	19.9	18.3	4.37	3.55	0.969
6.5	47.68	52.31	43.20	2.0924	0.335	110	0.286	25.5	20.6	32.3	3.69	3.47	1.37

pdf card number 98-062-9462. The crystal structure of pure copper is FCC and that of pure zinc is hexagonal. When the XRD patterns are evaluated in terms of pH change, it is seen that the diffraction peaks in the XRD patterns tend to increase with increasing pH value, although this trend seems to be broken in the sample produced at pH 5.5. The pH change affects the activity of citrate complexes which play a critical role in the reduction of Cu and Zn in the electrolyte. While some of the metal citrate species in the bath support the reduction, others may play an inhibitory role during the reduction.[25] It can be stated that metal citrate complexes, which play an effective role in the deposition of Zn content until pH 5.5, gradually increase their effect, but after pH 5.5, this effect starts to disappear. Especially pH 5.5 is a turning point in terms of Zn content. The change in peak height from pH 4.5 to 5 and the change in peak height from pH 5 to 5.5 are considered to be completely different situations. There is a phase change in the rise from pH 4.5 to 5, but the rise from pH 5 to 5.5 appears to be a change within the same phase type. The metal citrate complex activities affected by the pH change seem to have caused such a change in both elemental content and crystal orientation. The increasing trend in the peaks with increasing pH is also reflected in the increase in grain size (Table I). When the coating contents, which is one of the most important factors affecting the XRD patterns, are examined, it is understood that the increase in Zn changes direction and tends to decrease after pH 5.5 and this is also reflected in the patterns. At pH higher than 5.5, it can be stated that the increase in Zn content in the coating is restrained in terms of bath kinetics. The complexity of the electrodeposition baths does not always allow a linear change in the experimental results obtained. For example, a small change in an important parameter such as pH can have very important repercussions on the results. Furthermore, since the production of electrochemical alloys is not a balanced deposition process, they do not follow the phase diagram in an absolute way, but it is possible to say that there is a general compliance with the relevant phase diagram.[58] Another point is that an increase in the pH of the electrolyte can increase the grain size of the deposit by decreasing the nucleation rate. In addition, an increase in pH may cause an increase in current efficiency up to a certain value depending on the content of the electrolyte.[29,59,60] Pawar *et al.*[45] reported that pH increase in the electrodeposition of Cd-Se thin films increases the film thickness, but after a certain pH value, the film thickness tends to decrease again. The grain size increasing effect of pH increase seems to be generally consistent with XRD results. Table I shows that the crystalline grain size values calculated from the most intense peaks of the alloy films tend to increase with increasing pH. It is seen that the crystal grain size values of Cu–Zn alloys vary between ~ 14 and 25 nm. When the crystal grain size values are analyzed according to the pH change, the striking point is the sudden increase in the crystal grain size, especially in the transition from pH 4.5 to pH 5.0, and it seems possible to explain this situation with the transition

from α phase to β′ phase. With this pH increase, the nature of the electrolyte is affected and the properties of the resulting Cu–Zn alloy, such as crystal and phase structure, elemental content, *etc.*, may change; moreover, this change seems to have affected the nucleation mechanism during deposition and caused a sudden change in grain size. With the further increase in pH value, the crystal grain size first decreased and then showed an increasing trend with the increase in pH. It is noticeable that the effect of the change in Zn content on the change in crystal grain size seen after pH 5.0 is great. In Table I, there is an inverse relationship between the change in Zn content and the change in crystal grain size. It is seen in Table I that while the crystal grain size decreases with the increase in Zn content, the crystal grain size increases again with the decrease in Zn content. In addition, when the microstrain values (belongs to the highhest peak) given in Table I are examined, it is noticed that there is a sudden decrease with the transition of the phase structure from α to β′ phase with the increase in pH, and then follows a parallel change course with the Zn content affected by the pH change. When the grain size values calculated from the W–H graphs given in Table I and shown in Figure 6 are compared with the grain size values calculated by the Debye–Scherrer equation, it can be stated that the values are in general agreement. There is a slight difference between the microstrain values calculated from W–H plot and those calculated from Eq. [1], which are also shown in Table I. It is seen that the microstrain values calculated by the W–H plot method are lower than those obtained from Eq. [1]. Similarly in the literature, it is seen that there are similar differences in the microstrain values calculated by these two methods.[35,61]

Table II shows the effect of pH variation on the relative texture coefficient (RTC) values of Cu–Zn alloy coatings. XRD pattern of the β′ phase of Cu_1–Zn_1 alloys with reference code 98-062-9462 was used to calculate the RTC values. The Cu–Zn coating sample produced at pH 4.5 could not be included in the RTC calculations because it was in the α phase due to its low Zn content. From the RTC values in the table, it is observed that although there is a random orientation in general, the preferential orientation tends to be slightly concentrated in the (110) plane. It is found that with the increase in pH, the RTC values of the (110) plane decrease and the orientation in this plane shifts to the (200) and (211) planes. At pH 5.5, the orientation of the (200) plane is completely reflected in the (110) and (211) planes. At pH 5.5, the Zn content reached its maximum value and started to decrease at higher pH values and this turning point seems to have affected the crystal orientation of the phase structure. With the further increase in pH, the RTC values of the (200) plane reappeared and increased, while the RTC values in the (110) and (211) planes decreased with this effect. The contribution to the preferred orientation of the formation of the lowest overall energy conditions between the surface and strain energies of electrodeposited films can be expressed in terms of the principle of satisfying thermodynamic requirements. The film will tend to grow in whichever preferred orientation has the lowest surface or strain energy. From the RTC values, it is possible to state that the energy barrier level of this plane increases due to the relative decrease in orientation in the (110) plane with increasing pH. In addition, although pH increase decreases the energy level in the (200) plane, the situation in the (211) plane seems to be more complicated. With the increase in pH (5 to 5.5), the energy barrier level decreased with the effect of the phase change and the orientation in this plane increased significantly, but at higher pH values, the changing crystal structure conditions with the effect of complex electrodeposition kinetics seem to increase the energy level required for orientation in this plane. Changes in pH, an important electrochemical parameter, affect the bath conditions, thus causing changes in the elemental content of the coating. Basically, these content changes can have effects on properties such as phase structure, crystal structure, and preferred orientation. These effects can change the thermodynamic energy barrier values of the crystal orientation planes.[62–65]

C. *Morphology and Content Analysis*

In Figure 7, Cu and Zn contents in Cu–Zn thin films deposited at different electrolyte pH values are presented comparatively. Figure 8 shows the surface morphology and EDS graphs of Cu–Zn thin films produced at different bath pH values. The thicknesses of the Cu–Zn coatings produced were measured with a micrometer by peeling from the substrate and thickness values ranging between 6 and 10 μm were obtained. It was observed that there was no meaningful change between pH variation and coating thicknesses. The pH change can decrease the deposition rate of one of the elements that make up the alloy, while increasing the deposition rate of the other element.[25] Probably due to this reason, there may not be a significant change in coating thicknesses. It was also found that the coatings adhered very well to the substrates during stripping. Processes such as polishing and sanding performed before deposition are critical for the adhesion of the coatings to the substrate. It has been observed that the processes applied meticulously before deposition are effective in the adhesion of Cu–Zn coatings to the substrate. From Figure 7, it is evident that the bath pH values significantly affect the coating content. The Zn content first increased with increasing pH, but showed a decreasing trend after pH 5.5. Bedir *et al.*[66] investigated the effect of bath pH on the properties of Zn-Mn electroplatings and similarly reported that the Mn content in the alloy coating first increased with increasing pH, but after pH 5, the Mn content tended to decrease. The lowest Zn content was obtained in the film deposited at pH 4.5. It appears that the increased H^+ ions due to the relatively low pH value significantly inhibit the rate of incorporation of Zn ions into the coating. Since the pH scale is logarithmic, even small increases can significantly affect the nature of the electrolyte. In CV analyses, it was stated that the addition of sodium citrate brought the deposition potentials of Cu and Zn elements closer to each other and contributed to alloy deposition.[49]

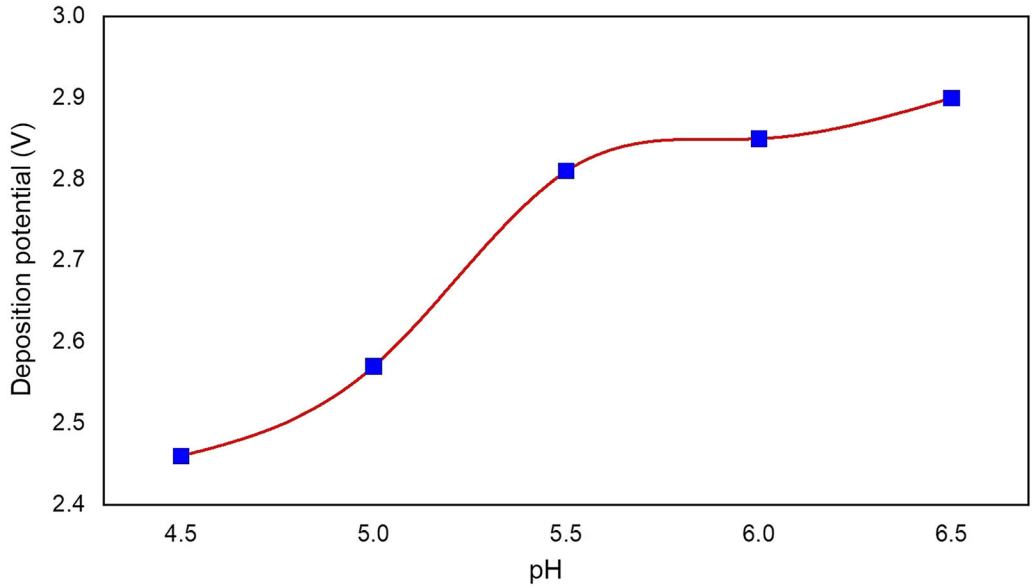

Fig. 4—Effect of electrolyte pH on the deposition potential of Cu–Zn coatings.

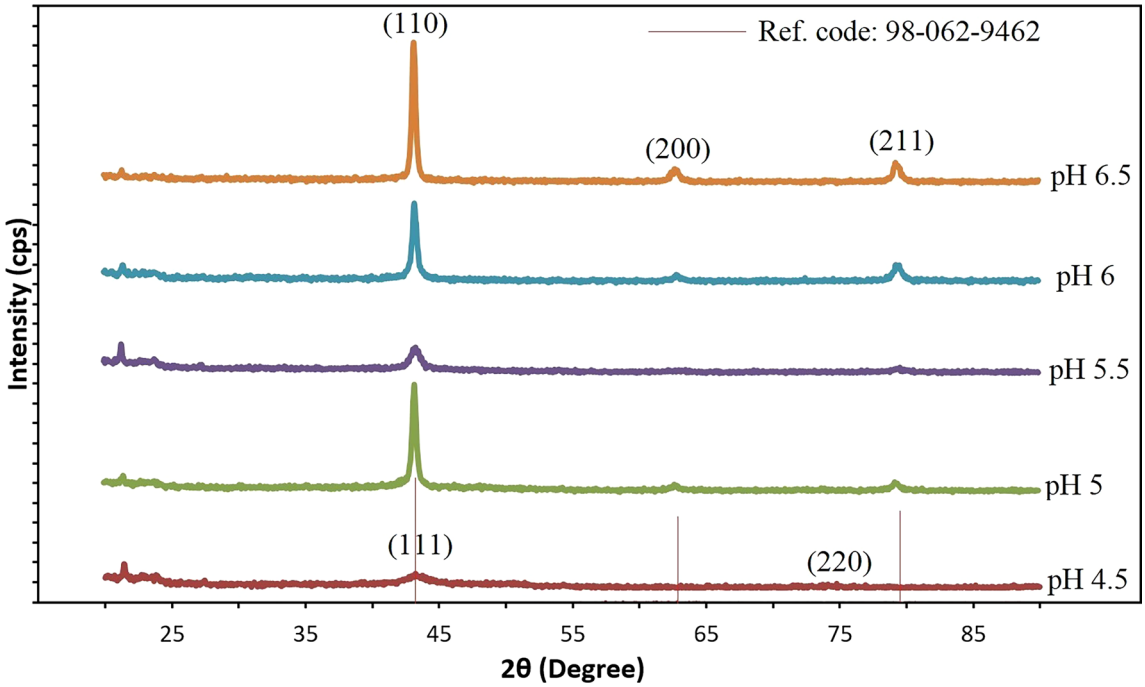

Fig. 5—XRD patterns of Cu–Zn films deposited at different electrolyte pH values.

However, it can be stated that the low pH value plays an inhibitory role in this effect of sodium citrate. Özdemir and Karahan[67] investigated the effect of sodium citrate on Cu–Zn alloys (deposited at pH 5.8) and found a similar situation in their study. According to the results obtained by the authors, it was observed that almost only Cu was deposited in the bath where sodium citrate was not added. It is clear from this that sodium citrate is critical for the deposition of Cu and Zn together and that the pH value must be appropriate for this effect to occur. Chassaing and Quang[68] stated that the pH value increased gradually with increasing citrate concentrations in the bath and this increase was due to the gradual neutralization of hydrogenated citrate ions. In our study, citrate concentration is constant, but changing pH values affect citrate ions. From the SEM images of Cu–Zn films in Figure 8, it can be stated that increasing the pH value greatly affects the surface appearance and structure. First of all, it can be easily noticed that the SEM image of the film produced at pH 4.5 with high Cu content has a darker color tone than the films produced at other pH values. It is understood that a dark color is

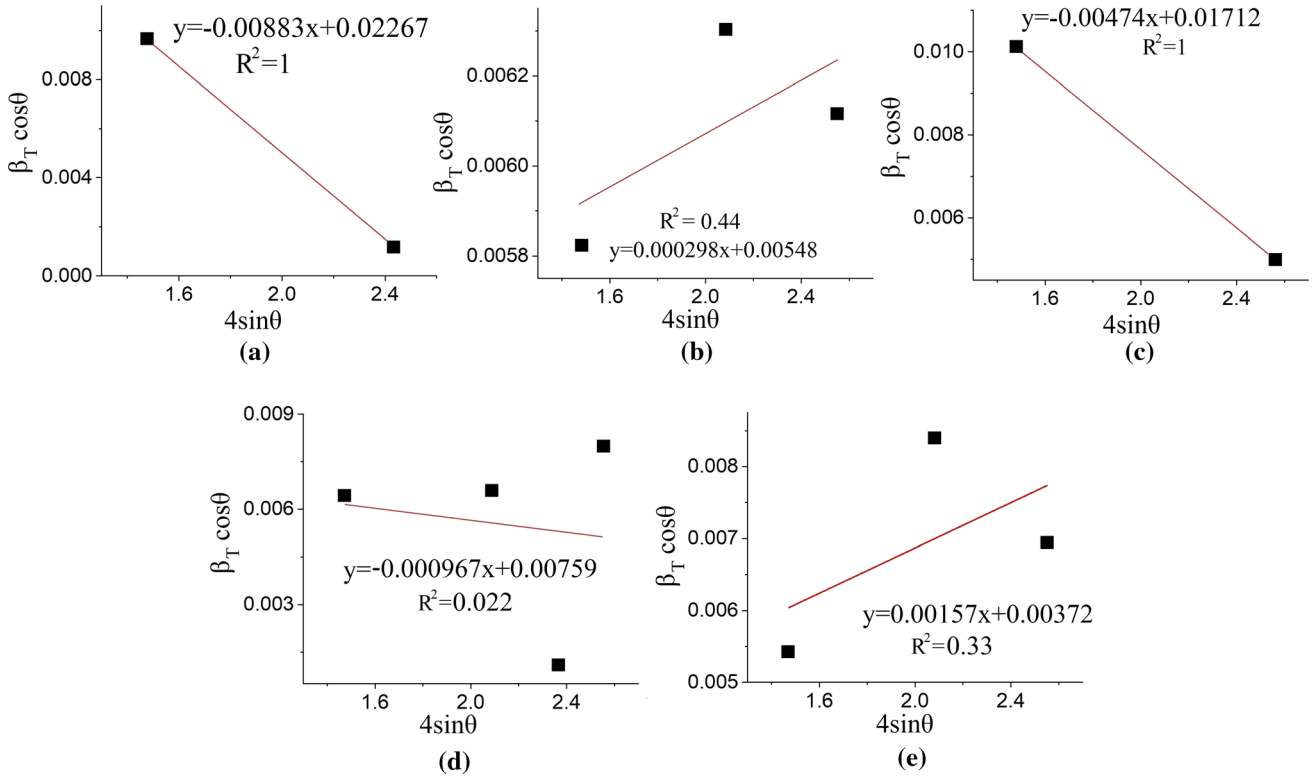

Fig. 6—W–H plot of Cu–Zn films deposited at different electrolyte pH values (*a*) 4.5, (*b*) 5, (*c*) 5.5, (*d*) 6, (*e*) 6.5.

obtained in this way due to the high Cu content. With the increase in the pH ratio and the increase in the Zn content, the color tone in the SEM images of the coatings changed toward white. This situation stands out as a determination compatible with the increase in the Zn content in the film content. Another noteworthy point in the SEM images is the decrease in the lateral gaps between the Cu–Zn layers that grow during the electrodeposition process with increasing pH value. Moreover, this seems to be more related to the pH value than the Zn content. Because, although the Zn content decreased after pH 6, the lateral gaps between the growing layers were completely closed and a denser and tighter Cu–Zn film was obtained at pH 6.5. The pH increase played an active role in the closure of the gaps by affecting the lateral growth capacity as well as the vertical growth of the Cu–Zn layers growing on the substrate. It can be stated that the effect of pH increase on increasing the grain size by decreasing the nucleation rate and the decrease of these lateral voids are mutually supportive.[29,59,60] Ibrahim and Bakdash[17] used glutamate as a complexing agent in their study on Cu–Zn alloy electrodeposition and investigated the effect of pH (in the range of 0–2.5) on the surface morphology of the coatings. The authors reported that at low pH values (0 and 1), Cu–Zn deposits were in the form of needles scattered on the substrate surface. In addition, they reported that as the pH value increased, Cu–Zn deposits started to cover the entire substrate surface and started to turn into cauliflower morphology to a great extent. In another study on Zn–Fe–Mo alloy deposition, Winiarski *et al.*[50] investigated the pH effect (4.8 to 6) on the surface morphology of the coatings. The authors reported that Zn–Fe–Mo coatings became more homogeneous, smooth and dense with increasing pH, but crack formation was observed with further increase in pH.

In the electrochemical deposition of polycrystalline metallic alloys, the process consists of nucleation and growth of these nuclei. The course of this process affects the morphology of the films and the size and shape of the grains. With the applied current, a certain number of nuclei are formed, which act as accumulation centers for atoms, and the nucleation and growth mechanisms occur simultaneously. The number of nuclei formed during the electrodeposition process and the deposition rate significantly influence each other. Depending on the rate of diffusion of atoms and electrodeposition production variables, new nuclei are formed, while already formed nuclei expand and continue to grow until equilibrium is reached. As conditions change, the structure of the film changes to adapt to the new conditions.[69,70]

D. *Electrical Resistivity Analysis*

In metals, electrical conduction is carried out by free electrons, which must be excited to free energy levels above the Fermi energy level to contribute to conduction. Metals have high electrical conductivity because a large number of electrons can fulfill this condition. Free electrons in metals move on average in the direction opposite to the current direction during scattering. The average distance over which free electrons can move in a

straight line without scattering is called the mean free path, and a lower mean free path results in higher electrical resistance. Resistance to the applied electric current can be explained by the presence of an effect called frictional forces. These frictional forces are due to factors such as the type and amount of impurity atoms, lattice stresses and vacancies, intermediate atoms, dislocation density, texture structure, the phase composition and type of alloy, and even the scattering of electrons caused by the thermal vibrations of the atom itself. Each scattering event causes the kinetic energy of the electron to decrease and the direction of motion to change. The scattering of electrons can be expressed as resistance to the passing electric current. When an impurity atom dissolves in a metal, it causes a redistribution of conduction electrons around the impurity atom. In addition, the crystal structure and grain size also affect the electrical resistivity of the material. In a given volume of material, the smaller the grain size, the greater the amount of intergranular boundary in that volume. Since grain boundaries act as scattering centers for electrical charge carriers, they contribute to the increase in electrical resistance.[53,69,71–73]

Figure 9 shows the effect of temperature change between 149 K and 395 K (− 122 °C to 122 °C) on the electrical resistivity values of Cu–Zn alloys deposited at different electrolyte pH values. Figure 10 shows the effect of the pH change of the electrolytes in which the deposition process was carried out on the electrical resistivity values of Cu–Zn alloys at different temperatures. From the data obtained, it is concluded that the electrical resistivity values of Cu–Zn alloy films vary between 0.0305 and 0.0828 $\mu\Omega$cm. When the graphs given in Figures 9 and 10 are evaluated together, first of all, it is seen that the electrical resistivity values of all Cu–Zn alloys increase steadily with the increase in temperature. In pure metals and most Cu alloys, resistivity increases linearly with temperature. In metallic materials, the thermal energy increase in the crystal structure with increasing temperature leads to an increase in lattice vibrations. This effect leads to an increase in the scattering of charge carriers (phonon scattering of conduction electrons) and thus to an increase in the electrical resistivity of the metallic material.[53,69] Miyajima *et al.*[73] performed electrical resistance measurements of Cu–Zn alloys with approximately 31 pct Zn content at temperatures of 77 K and 293 K. According to the results obtained by the authors, the electrical resistance of Cu–Zn alloy increased more than 5 times with increasing temperature.

Table II. Effect of pH on RTC Values of Cu–Zn Coatings

Sample	RTC $_{(110)}$	RTC $_{(200)}$	RTC $_{(211)}$
pH 5	59.85	22	18.15
pH 5.5	56.11	0	43.9
pH 6	42.22	23.5	34.24
pH 6.5	46.41	28.57	25.02

When the effect of electrolyte pH change on electrical resistivity is examined from Figures 9 and 10, it is apparent that the resistivity first increases with pH increase and then decreases again after pH 5.5. pH 5.5 appears to be a turning point in electrical resistivity values, as well as a turning point in terms of Cu and Zn content in the coating, crystal grain size, and change in RTC values (see Tables I and II, Figure 7). These three factors are potential properties that can affect the electrical resistivity and all of them were affected by the electrolyte pH change. While the electrical resistivity increased with decreasing Cu content and increasing Zn content in Cu–Zn films, the decrease in Zn content after pH 5.5 had an effect on the decrease in resistance value. This can be explained by the contribution of empurite atoms to the electrical resistivity. Fairbank[74] studied the electrical resistivity properties of Cu–Zn alloys from 14 K to room temperature and reported that the resistivity of the material increases with the increase in Zn content in the alloy. The change in crystal grain size also seems to be effective on resistivity, especially after pH 5.5, the crystal grain size tends to increase, which may play a role in the decrease in resistivity. The change in the RTC values calculated from the XRD patterns of Cu–Zn alloys is also one of the factors that may be effective on the resistivity, and it should not be ignored that the fact that there is no XRD reflection at pH 5.5, especially in the (200) plane, and the maximum value of the RTC value in the (211) plane may be an effective factor in obtaining the maximum resistivity value. Because crystal lattice orientation is one of the highly influential factors in terms of the movement of charge-carrying electrons. It is visible that RTC values belonging to the (200) plane are present at values lower and higher than pH 5.5 (Table II). Lakshya *et al.*[75] investigated the relationship between the relative texture coefficient of a ceramic material and its electrical resistance. According to the authors, the electrical resistance increased up to 40 times with a 200 pct increase in the texture coefficient. Another important issue that can affect the electrical resistance of Cu–Zn alloys is the phase structure. In particular, Cu–Zn coatings produced at pH 4.5 were in the α phase, while at higher pH values there was a transition to the β' phase. It is revealed from Figures 9 and 10 that the lowest resistivity value is in the α phase sample produced at pH 4.5. It is clearly understood from the graphs that the resistivity values of the other samples in the β' phase are relatively higher. Ayers and Massalski[76] investigated the electrical resistivity values of α and β phases of Cu–Zn alloys and reported that the β phase exhibited higher resistivity values than the α phase. In another study, Miyajima *et al.*[73] investigated the effect of rolling process on the electrical resistance of Cu–Zn alloys with Cu content around 70 pct. The authors stated that as a result of this process, the electrical resistance also increased due to the heterogeneous nanostructure due to the increased grain boundary and dislocation density. The authors also noted that the electrical resistivity increases as a result of a decrease in the mean free path of electrons with increasing density of lattice defects caused by rolling.

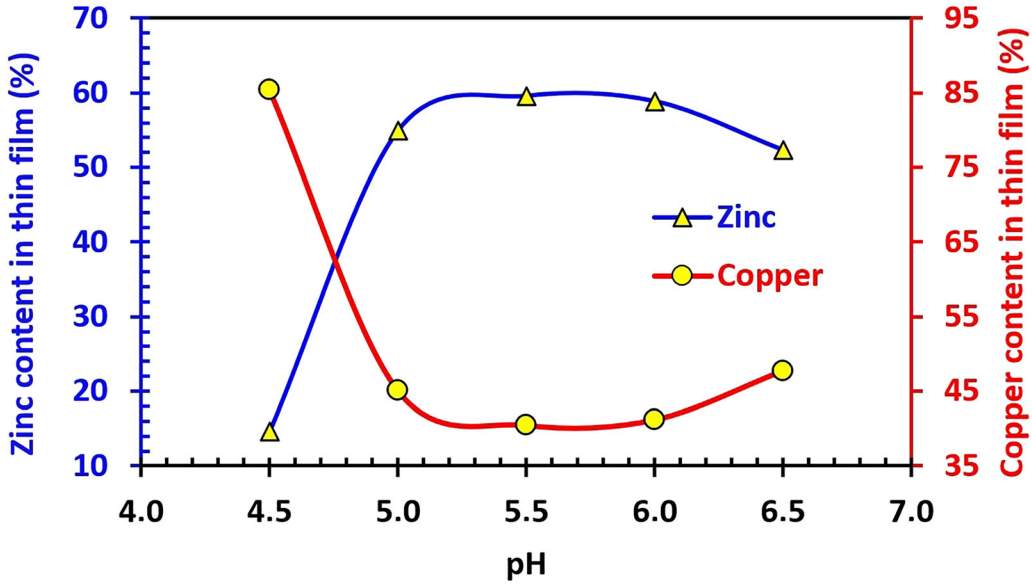

Fig. 7—Variation of copper and zinc content in Cu–Zn thin films according to bath pH effect.

E. *DSC Analysis*

The DSC curves of Cu–Zn alloys deposited at different electrolyte pH values in the range of 0 °C to 400 °C are presented together in Figure 11. The figure shows that the endothermic energy flow is more pronounced up to around 250 °C, while the energy flow decreases much more after 250 °C. Particularly in the range 150 °C to 250 °C, pronounced endothermic peaks are observed. These energy transitions up to around 250 °C are thought to be related to possible phase formation and transformations. In addition, it should be taken into consideration that the processes of phase irregularity elimination with thermal energy input to the material may also take place in this range.[77,78] First of all, it should be noted that since electrodeposition of Cu–Zn alloys is not a balanced deposition process, the phase diagrams may not be in complete agreement.[58] Cu–Zn alloys with less than 60 pct Zn content can have α, β' and γ phases at room temperature at different rates according to their content values. However, since there may not be sufficient conditions for the diffusion of atoms during the electrodeposition process, a complete phase formation may not occur according to the element content. When electrodeposited Cu–Zn alloys are heated, the Cu and Zn elements that make up the alloy can undergo phase formation or transformations in order to reach equilibrium. In this case, when Cu–Zn alloys are exposed to heat, the structure of the alloy can be rearranged by diffusion of Zn atoms. In Cu–Zn alloys, the transformation from the γ phase to the β' phase can take place at temperatures around 200 °C to 300 °C.[79,80] The endothermic peaks seen in Figure 11 are likely to involve the transformation of the γ or α phases in the structure into the β' phase as well as the diffusive rearrangement of atoms to reach equilibrium.[77–79] Hu *et al.*,[77] performed DSC analyses of Ni–Mo alloys on electrodeposited samples and annealed samples at different temperatures for 1 hours (700 °C, 1000 °C, 1200 °C). The authors reported that the peaks in the DSC curves of the electrodeposited samples are depressed peaks that spread over a wider temperature range compared to the annealed samples. The authors also noted that more energy release occurs in the DSC curves of electrodeposited Ni–Mo alloys compared to annealed ones. In another study, Kapoor *et al.*[78] performed DSC analysis on the amount of energy stored in crystallographic defects of nanocrystalline Ni–Mo coatings produced by electrodeposition method. The authors state that most of the heat released in DSC analysis is due to grain coarsening and the elimination of dislocations and twin faults. The authors also stated that the energy stored doubled with the increase in Mo content from 0.4 to 5.3 pct in the alloy coating, which is caused by higher crystal defect density and finer grain structure. The heights of the endothermic peaks at pH 4.5, 5, and 5.5 appear to be the same, but at pH 5 and 5.5, the possible phase formation and transformations started at lower temperatures; and moreover, at pH 5 the peak ended at lower temperatures. The height of the peak at pH 6 has increased and the starting and ending temperatures of the peak appear wider. In this case, it is thought that more phase transformation or formation processes occur in the sample produced at pH 6. At pH 6.5, no significant endothermic peak is observed, but it is clear from the DSC curve that a certain level of heat transfer occurs up to around 250 °C. Due to the deposition conditions at this value, it is understood that the amount of possible phase transformation or formation is relatively reduced in this temperature range. Due to the relatively low Zn content in this sample deposited at pH 6.5, it is thought that the γ phase is not present at all or not in an amount that could cause an endothermic peak. Pan *et al.*[79] reported that in their DSC analysis of Cu–Zn alloy with 40 pct Zn content, the endothermic peak in the transformation from γ phase to β' phase starts around 250 °C and lasts until around 400 °C. The

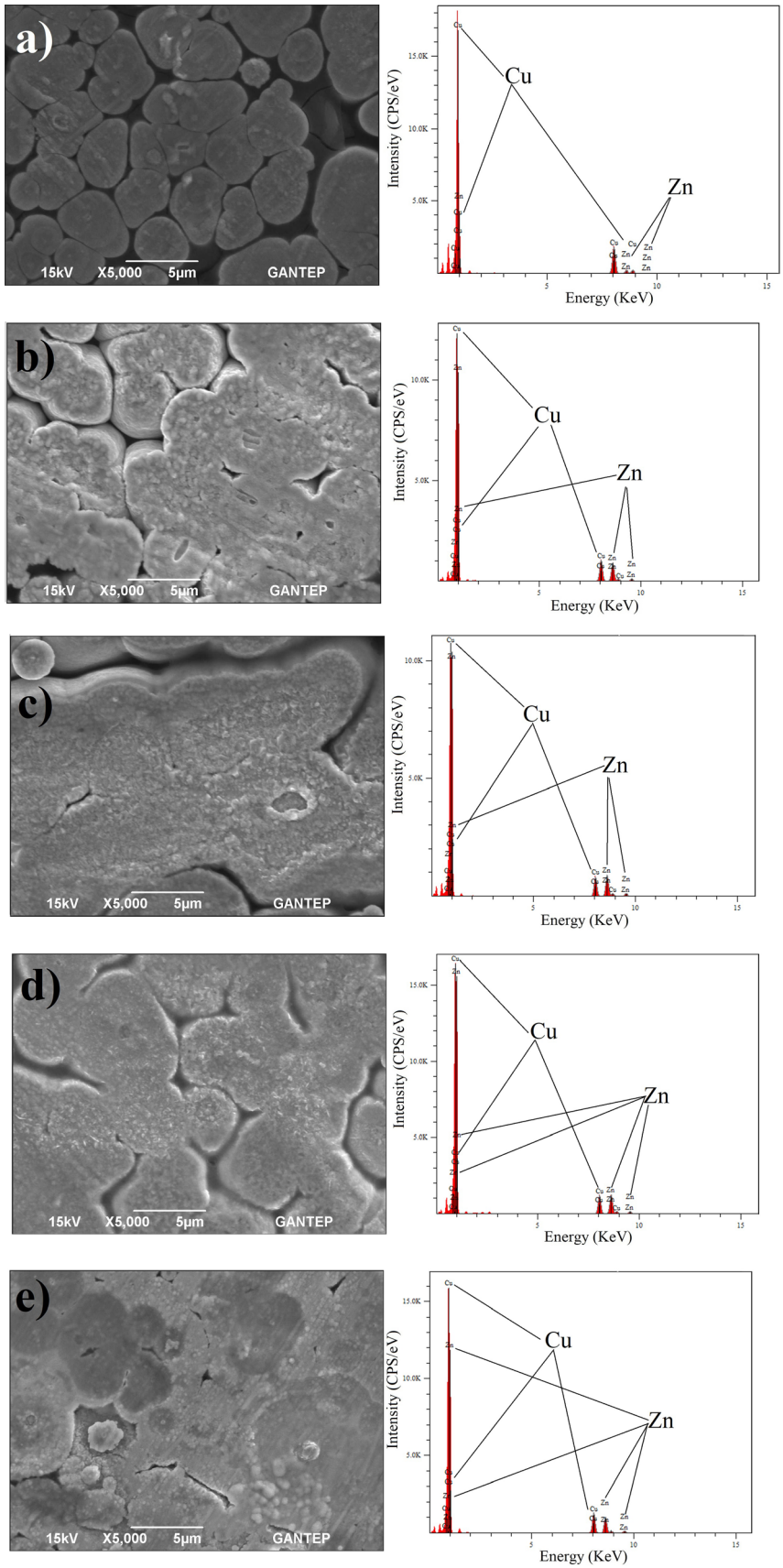

Fig. 8—Surface structure and EDS graphs of Cu–Zn thin films obtained at different bath pH values (*a*) pH 4.5, (*b*) pH 5, (*c*) pH 5.5, (*d*) pH 6, (*e*) pH 6.5.

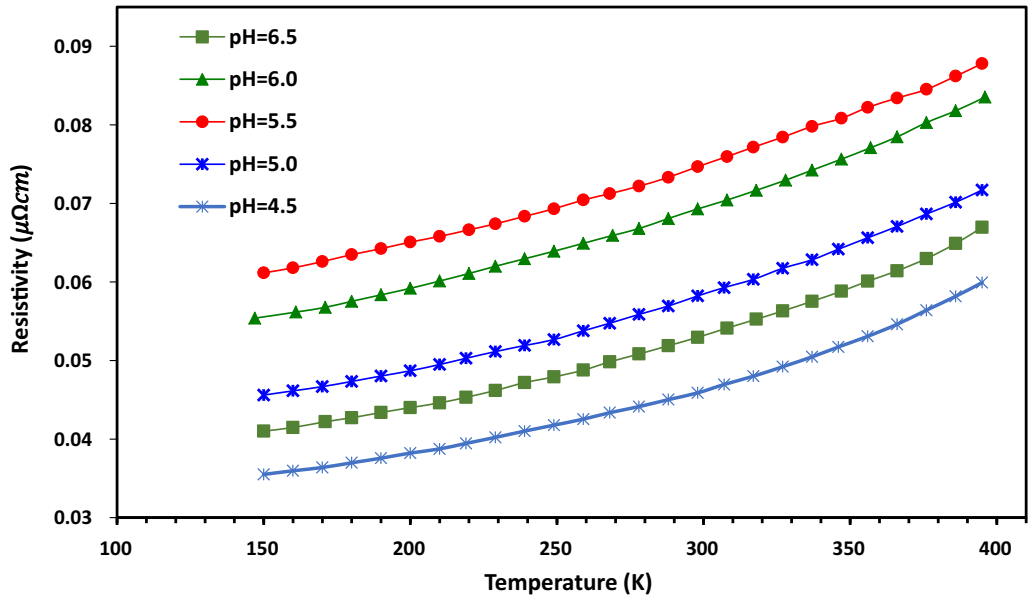

Fig. 9—Effect of temperature variation on electrical resistivity values of Cu–Zn alloys at different electrolyte pH values.

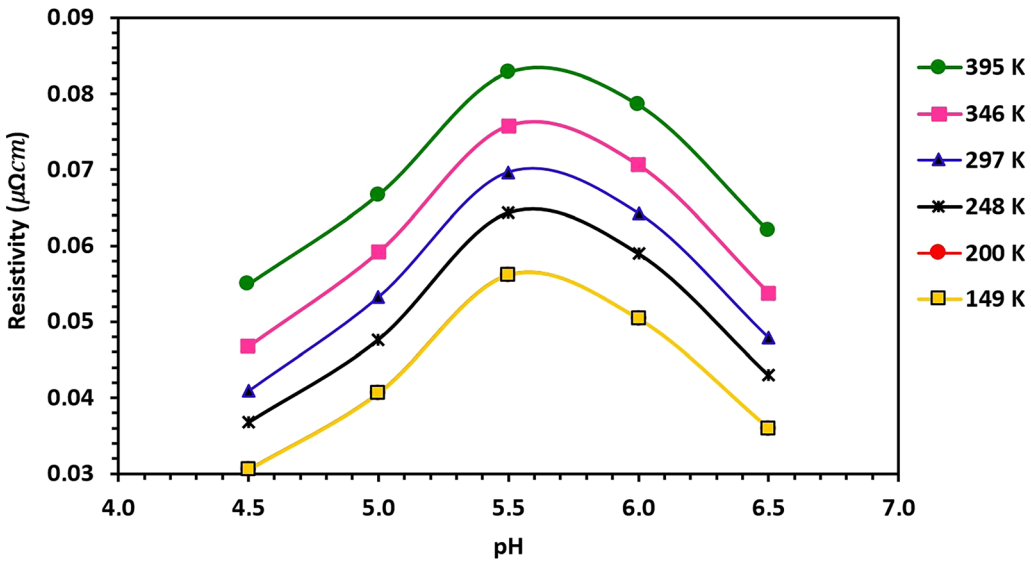

Fig. 10—The effect of the pH change of the electrolytes in which the deposition process is carried out on the electrical resistivity values of Cu–Zn alloys at different temperatures.

authors also reported that at temperatures above 400 °C, the transformation from the β' phase to the β phase begins. In another study, Mannan *et al.*[81] stated that the transformation temperature from β' phase to α and γ phases in Cu–25 pctZn–6 pct Al alloys starts at around 430 °C and ends at around 330 °C.

IV. CONCLUSION

Cu–Zn alloys were coated on aluminum substrate for 60 minutes at a current density of 8 mA/cm^2 by electrodeposition method. The effect of different bath pH values (4.5 to 6.5) on various properties of the obtained coatings was investigated. In addition, the behavior of the electrolytes at different pH values was analyzed by CV method. The results obtained are listed below.

– From the CV analysis, it is seen that pH increase causes a negative shift in the deposition potential of Cu–Zn alloys up to pH 5.5, while there is no further negative shift at higher pH values. The rate of increase in current density in the cathodic direction increased up to pH 5.5 and started to decrease again

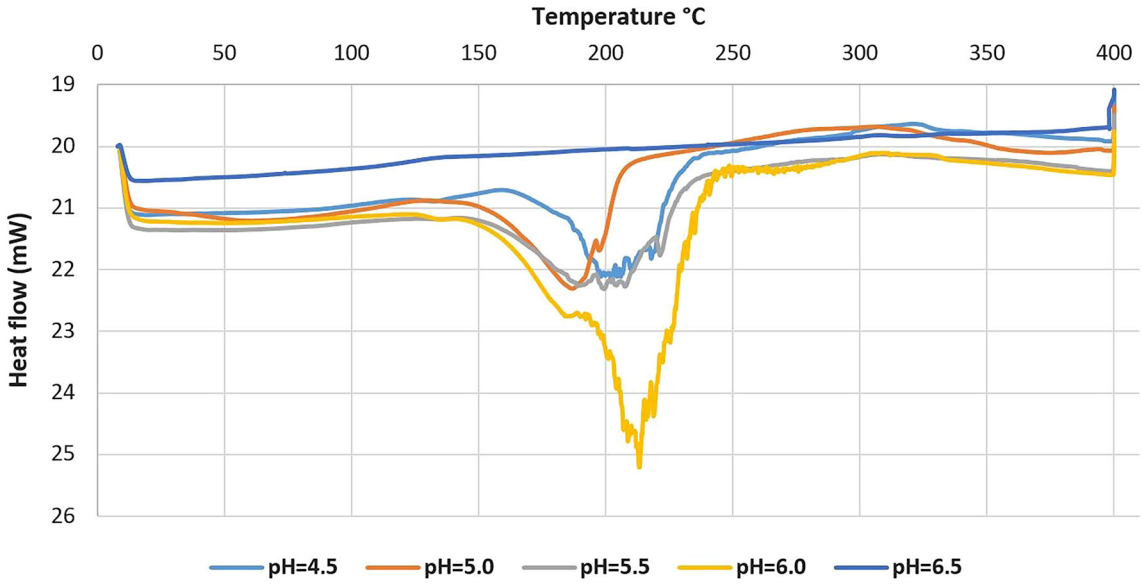

Fig. 11—DSC curves of Cu–Zn alloys deposited at different electrolyte pH values.

at higher values. Similar situation is observed in the dissolution peak heights in the anodic direction. In addition, the pH increase caused an increase in the deposition potential of Cu–Zn alloys.

- The Cu–Zn film produced at pH 4.5 was found to be α phase, while the alloy films produced at pH 5, 5.5, 6, 6.5 were generally composed of β' phase. The crystal grain size values of the films increased relatively with increasing pH and the microstrain values first decreased and then followed a horizontal course.
- With increasing pH, the Zn content in Cu–Zn alloys first increased and then showed a slight decreasing trend after a horizontal course. In addition, the pH increase contributed positively to the lateral growth processes of the Cu–Zn alloy layers growing on the cathode surface, resulting in a denser coating.
- The electrical resistivity values of Cu–Zn alloy films ranged from 0.0305 to 0.0828 $\mu\Omega$cm. The electrical resistivity values first increased with increasing pH and then showed a decreasing trend. In addition, the resistivity values of Cu–Zn alloys also increased with increasing temperature.
- The endothermic peaks observed between 150 °C and 250 °C in DSC analyses are thought to cover the transformation of γ phases in the structure into β' phase as well as the diffusive rearrangement of atoms and phase formation processes to reach equilibrium. With the pH change, the heights of the endothermic peaks and the starting and ending temperatures also changed.

FUNDING

Open access funding provided by the Scientific and Technological Research Council of Türkiye (TÜBİTAK).

CONFLICT OF INTEREST

On behalf of all authors, the corresponding author states that there is no conflict of interest.

OPEN ACCESS

REFERENCES

1. M.S. Safavi and A. Rasooli: *J. Mater. Res. Technol.*, 2024, vol. 28, pp. 865–78. https://doi.org/10.1016/j.jmrt.2023.12.014.
2. E. Ünal, A. Yaşar, and İH. Karahan: *Metall. Mater. Trans. A*, 2023, vol. 54A, pp. 2340–61. https://doi.org/10.1007/s11661-023-07020-0.
3. M.K. Kolle, S. Shajahan, and A. Basu: *Metall. Mater. Trans. A*, 2020, vol. 51A, pp. 3721–31. https://doi.org/10.1007/s11661-020-05787-0.
4. S.I. Ghazanlou, A.H.S. Farhood, S. Ahmadiyeh, E. Ziyaei, A. Rasooli, and S. Hosseinpour: *Metall. Mater. Trans. A*, 2019, vol. 50A, pp. 1922–35. https://doi.org/10.1007/s11661-019-05118-y.
5. J. Chen, C. Ruffert, H.H. Gatzen, R. Bandorf, and G. Brauer: *Design and Manufacturing of Active Microsystems*

Microtechnology and MEMS, Springer, Berlin, 2011, pp. 167–88. https://doi.org/10.1007/978-3-642-12903-2_10.
6. İH. Karahan and R. Özdemir: *Appl. Surf. Sci.*, 2014, vol. 318, pp. 100–04. https://doi.org/10.1016/j.apsusc.2014.01.119.
7. M. Abdolmaleki, K. Ghamari, S. Ahmadiyeh, B. Azadi, Y. Hanifehpour, G.L. Allahgholipour, J. Hosseini, and A.H.S. Farhood: *Metall. Mater. Trans. A*, 2024, vol. 55A, pp. 352–59. https://doi.org/10.1007/s11661-023-07253-z.
8. A.P. Meshram, A. Gupta, and C. Srivastava: *Metall. Mater. Trans. A*, 2022, vol. 53A, pp. 1430–39. https://doi.org/10.1007/s11661-022-06603-7.
9. A.H. Noorbakhsh Nezhad, E. Mohammadi Zahrani, and A.M. Alfantazi: *Corros. Sci.*, 2022, vol. 197, p. 110095. https://doi.org/10.1016/j.corsci.2022.110095.
10. J. Zhu: *Appl. Surf. Sci.*, 2018, vol. 447, pp. 363–67. https://doi.org/10.1016/j.apsusc.2018.04.014.
11. H.J. Choi, J.H. Shin, S. Choo, S.W. Ryu, Y.D. Kim, and H. Lee: *Thin Solid Films*, 2015, vol. 585, pp. 76–80. https://doi.org/10.1016/j.tsf.2015.03.046.
12. L. Feng, H. Zhang, Z. Wang, and Y. Liu: *Colloids Surf A*, 2014, vol. 441, pp. 319–25. https://doi.org/10.1016/j.colsurfa.2013.09.014.
13. S. Lee, J. Hong, C. Xu, M. Lee, D. Kim, L. Lin, W. Hwang, and Z.L. Wang: *Adv. Mater.*, 2012, vol. 24, pp. 4398–4402. https://doi.org/10.1002/adma.201201525.
14. S. Ghanbari and F. Mahboubi: *Mater. Des.*, 2011, vol. 32, pp. 1859–64. https://doi.org/10.1016/j.matdes.2010.12.020.
15. C. Oulmas, S. Mameri, D. Boughrara, A. Kadri, J. Delhalle, Z. Mekhalif, and B. Benfedda: *Heliyon*, 2019, vol. 5, p. e02058. https://doi.org/10.1016/j.heliyon.2019.e02058.
16. R. Özdemir and İH. Karahan: *Appl. Surf. Sci.*, 2014, vol. 318, pp. 314–18. https://doi.org/10.1016/j.apsusc.2014.06.188.
17. M.A.M. Ibrahim and R.S. Bakdash: *Surf. Interfaces*, 2020, vol. 18, p. 100404. https://doi.org/10.1016/j.surfin.2019.100404.
18. C.S. Lin, H.B. Lee, and S.H. Hsieh: *Metall. Mater. Trans. A*, 2000, vol. 31A, pp. 475–85. https://doi.org/10.1007/s11661-000-0283-z.
19. S. Staroń, P. Ledwig, and B. Dubiel: *Metall. Mater. Trans. A*, 2022, vol. 53A, pp. 2071–85. https://doi.org/10.1007/s11661-022-06649-7.
20. S.U. Rehman, M. Khan, A.N. Khan, L. Ali, and S.H.I. Jaffery: *Acta Phys. Pol. A*, 2015, vol. 128, pp. 125–27. https://doi.org/10.12693/APhysPolA.128.B-125.
21. Y. Fu, H. Du, W. Huang, S. Zhang, and M. Hu: *Sens. Actuators A*, 2004, vol. 112, pp. 395–408. https://doi.org/10.1016/j.sna.2004.02.019.
22. X. Ren and K. Otsuka: *MRS Bull.*, 2002, vol. 27, pp. 115–20. https://doi.org/10.1557/mrs2002.47.
23. K. Yurdal and İH. Karahan: *Acta Phys. Pol. A*, 2017, vol. 132, pp. 1091–94. https://doi.org/10.12693/APhysPolA.132.1091.
24. S.M.A. Mousavi and R. Pitchumani: *Corros. Sci.*, 2021, vol. 186, p. 109420. https://doi.org/10.1016/j.corsci.2021.109420.
25. A. Dridi, L. Dhouibi, J. Hihn, P. Berçot, W. Sassi, and M. Rezrazi: *J. Electrochem. Soc.*, 2020, vol. 167, p. 062508. https://doi.org/10.1149/1945-7111/ab819b.
26. A. Kahoul, F. Azizi, and M. Bouaoud: *Trans. IMF*, 2017, vol. 95, pp. 106–13. https://doi.org/10.1080/00202967.2017.1265766.
27. T.A. Green, A.E. Russell, and S. Roy: *J. Electrochem. Soc.*, 1998, vol. 145, pp. 875–81. https://doi.org/10.1149/1.1838360.
28. İH. Karahan: *Optoelectron. Adv. Mat.*, 2008, vol. 2, pp. 828–32.
29. S.M.S.I. Dulal, H.J. Yun, C.B. Shin, and C.-K. Kim: *Electrochim. Acta*, 2007, vol. 53, pp. 934–43. https://doi.org/10.1016/j.electacta.2007.08.006.
30. H. Kazimierczak and P. Ozga: *Surf. Sci.*, 2013, vol. 607, pp. 33–38. https://doi.org/10.1016/j.susc.2012.08.010.
31. H. Kazimierczak, P. Ozga, and R.P. Socha: *Electrochim. Acta*, 2013, vol. 104, pp. 378–90. https://doi.org/10.1016/j.electacta.2012.12.140.
32. I. Boukhoubza, M. Khenfouch, M. Achehboune, B.M. Mothudi, I. Zorkani, and A. Jorio: *J. Phys.*, 2019, vol. 1292, p. 012011. https://doi.org/10.1088/1742-6596/1292/1/012011.
33. Z.R. Khan, M. Zulfequar, and M.S. Khan: *Mater. Sci. Eng. B*, 2010, vol. 174, pp. 145–49. https://doi.org/10.1016/j.mseb.2010.03.006.
34. P. Bindu and S. Thomas: *J. Theoret. Appl. Phys.*, 2014, vol. 8, pp. 123–34. https://doi.org/10.1007/s40094-014-0141-9.
35. M. Basak, M.L. Rahman, M.F. Ahmed, B. Biswas, and N. Sharmin: *J. Alloys Compd.*, 2022, vol. 895(2), p. 162694. https://doi.org/10.1016/j.jallcom.2021.162694.
36. R. Vishwaroop and S.N. Mathad: *Sci. Sinter.*, 2020, vol. 52, pp. 349–58. https://doi.org/10.2298/SOS2003349V.
37. A. Tozar: *Surf. Eng.*, 2020, vol. 36, pp. 990–99. https://doi.org/10.1080/02670844.2020.1730628.
38. W. Gu, C. Liu, J. Tang, R. Liu, H. Yang, and J. Hu: *Hydrometallurgy*, 2018, vol. 175, pp. 43–51. https://doi.org/10.1016/j.hydromet.2017.10.030.
39. A. Yousif, V. Kumar, R.M. Jafer, and H.C. Swart: *Appl. Surf. Sci.*, 2017, vol. 424, pp. 407–11. https://doi.org/10.1016/j.apsusc.2017.01.001.
40. B. Szczygiel and A. Laszczynska: *Trans. IMF*, 2014, vol. 92, pp. 196–202. https://doi.org/10.1179/0020296714Z.000000000183.
41. F.I.L. Tzec, L.C. Canul, and G. Oskam: *Electrochim. Acta*, 2011, vol. 56, pp. 9391–96. https://doi.org/10.1016/j.electacta.2011.08.023.
42. S. Rode, C. Henninot, C. Vallieres, and M. Matlosz: *J. Electrochem. Soc.*, 2004, vol. 151(6), p. C405. https://doi.org/10.1149/1.1715092.
43. H. Kazimierczak, K. Szymkiewicz, L. Rogal, E. Gleadi, and N. Eliaz: *J. Electrochem. Soc.*, 2018, vol. 165(11), p. D526. https://doi.org/10.1149/2.0421811jes.
44. M. Ichante, Y. Vidal, F. Valenzuela, J. Ballesteros, E. Arciga, Ş Talu, A. Albores, and G. Trejo: *J. Electroanal. Chem.*, 2018, vol. 823, pp. 328–34. https://doi.org/10.1016/j.jelechem.2018.06.032.
45. S.M. Pawar, A.V. Moholkar, and C.H. Bhosale: *Mater. Lett.*, 2007, vol. 61, pp. 1034–38. https://doi.org/10.1016/j.matlet.2006.06.044.
46. A. Sharma, S. Bhattacharya, S. Das, and K. Das: *Metall. Mater. Trans. A*, 2014, vol. 45A, pp. 4610–22. https://doi.org/10.1007/s11661-014-2389-8.
47. D. Grujicic and B. Pesic: *Electrochim. Acta*, 2002, vol. 47, pp. 2901–12. https://doi.org/10.1016/S0013-4686(02)00161-5.
48. T.J. Kemp, *Instrumental Methods in Electrochemistry*, Southampton Electrochem. Group, Ellis Horwood Ltd, 1985.
49. S. Shin, C. Park, C. Kim, Y. Kim, S. Park, and J. Lee: *Curr. Appl. Phys.*, 2016, vol. 16, pp. 207–10. https://doi.org/10.1016/j.cap.2015.11.017.
50. J. Winiarski, A. Leśniewicz, P. Pohl, and B. Szczygieł: *Surf. Coat. Technol.*, 2016, vol. 299, pp. 81–89. https://doi.org/10.1016/j.surfcoat.2016.04.073.
51. S. Zhang, L. Lu, and M.O. Lai: *Mater. Sci. Eng. A*, 1993, vol. 171, pp. 257–62. https://doi.org/10.1016/0921-5093(93)90413-9.
52. T. Prasankumar, D.J. Kang, M. Kim, and H.T. Lim: *Int. J. Electrochem. Sci.*, 2023, vol. 18(10), p. 100315. https://doi.org/10.1016/j.ijoes.2023.100315.
53. W.D. Callister and D.G. Rethwisch: *Materials Science and Engineering*, 8th ed. Wiley, Hoboken, 2015.
54. D.G. Page: *Electrodeposition of Thin Film Shape Memory Alloys*. Doctor of Philosophy Degree, New Castle University Library, 2001.
55. I. Abacha and S. Boukhrissa: *Surf. Eng. Appl. Electrochem.*, 2018, vol. 54, pp. 459–67. https://doi.org/10.3103/S1068375518050022.
56. H. Li, S. Yu, J. Hu, and X. Yin: *Appl. Surf. Sci.*, 2019, vol. 481, pp. 872–82. https://doi.org/10.1016/j.apsusc.2019.03.123.
57. H.W. Pickering: *J. Electrochem. Soc.*, 1970, vol. 117, p. 8. https://doi.org/10.1149/1.2407450.
58. S.D. Beattie and J.R. Dahn: *J. Electrochem. Soc.*, 2003, vol. 150(11), p. C802. https://doi.org/10.1149/1.1615998.
59. H. Natter: *J. Phys. Chem.*, 1996, vol. 50, pp. 19525–32. https://doi.org/10.1021/jp9617837.
60. M.H. Seo, D.J. Kim, and J.S. Kim: *Thin Solid Films*, 2005, vol. 489, pp. 122–29. https://doi.org/10.1016/j.tsf.2005.05.011.
61. Y. Prabhu, K. Rao, V. Kumar, and B. Kumari: *World J. Nano Sci. Eng.*, 2014, vol. 4, pp. 21–28. https://doi.org/10.4236/wjnse.2014.41004.
62. Q. Bao, W. Zheng, L. Chen, Z. Xu, J. Han, and C. Zhu: *Colloids Surf A*, 2022, vol. 636, p. 128128. https://doi.org/10.1016/j.colsurfa.2021.128128.
63. J. Pelleg, L.Z. Zevin, S. Lungo, and N. Croitoru: *Thin Solid Films*, 1991, vol. 197, pp. 117–28. https://doi.org/10.1016/0040-6090(91)90225-M.

64. Y. Cheng, X. Zhao, W. Xia, Q. Yue, Y. Gu, and Z. Zhang: *Mater. Des.*, 2024, vol. 237, p. 112582. https://doi.org/10.1016/j.matdes.2023.112582.
65. D.R. McKenzie and M.M.M. Bilek: *Thin Solid Films*, 2001, vol. 382, pp. 280–87. https://doi.org/10.1016/S0040-6090(00)01702-8.
66. M. Bedir, D. Korkmaz, O.F. Bakkaloglu, M. Oztas, İH. Karahan, and M.Y. Haciibrahimoglu: *Int. J. Electrochem. Sci.*, 2015, vol. 10, pp. 4513–22. https://doi.org/10.1016/S1452-3981(23)06641-5.
67. R. Özdemir and İH. Karahan: *Prot. Met. Phys. Chem. Surf.*, 2023, vol. 59, pp. 445–52. https://doi.org/10.1134/S207020512370051X.
68. E. Chassaing and K.V. Quang: *J. Appl. Electrochem.*, 1986, vol. 16, pp. 591–660. https://doi.org/10.1007/BF01006854.
69. R. Özdemir and İH. Karahan: *Trans. IMF*, 2019, vol. 97, pp. 95–99. https://doi.org/10.1080/00202967.2019.1570738.
70. M.V. Tomić, M.M. Bučko, M.G. Pavlović, and J.B. Bajat: *Contemp. Mater.*, 2010, vol. 1, pp. 87–93.
71. P. Wissmann and H.U. Finzel: *Electrical Resistivity of Thin Metal Films*, 7th ed. Springer, New York, 2007. https://doi.org/10.1007/3-540-48490-6.
72. T. Farrell and D. Greig: *J. Phys. C*, 1963, vol. 1, p. 1359. https://doi.org/10.1088/0022-3719/1/5/326.
73. Y. Miyajima, H. Morimoto, M. Miyazaki, T. Okada, K. Ishikawa, C. Watanabe, and H. Miura: *Mater. Trans.*, 2022, vol. 63, pp. 484–88. https://doi.org/10.2320/matertrans.MT-D2021005.
74. H.A. Fairbank: *Phys. Rev.*, 1944, vol. 66, pp. 274–81. https://doi.org/10.1103/PhysRev.66.274.
75. A.K. Lakshya, L. Kumar, K. Kumar, and A. Chowdhury: *Mater. Lett.*, 1858, vol. 314, p. 13. https://doi.org/10.1016/j.matlet.2022.131858.
76. J.D. Ayers and T.B. Massalski: *Metall. Trans.*, 1972, vol. 3, p. 3185. https://doi.org/10.1007/BF02661332.
77. J. Hu, Y.-N. Shi, and K. Lu: *Scr. Mater.*, 2018, vol. 54, pp. 182–85. https://doi.org/10.1016/j.scriptamat.2018.05.036.
78. G. Kapoor, L. Péter, É. Fekete, J.L. Lábár, and J. Gubicza: *J. Alloys Compd.*, 2019, vol. 796, pp. 307–13. https://doi.org/10.1016/j.jallcom.2019.05.032.
79. S. Pan, G. Yao, M. Sokoluk, Z. Guan, and X. Li: *Mater. Des.*, 2019, vol. 180, p. 107964. https://doi.org/10.1016/j.matdes.2019.107964.
80. H. Lee, I. Lee, X. Xu, T. Omori, R. Kainuma, and J. Ph: *Equilibria Diff.*, 2023, https://doi.org/10.1007/s11669-023-66601061-z.
81. S.K. Mannan, V. Ganesan, M. Vijayalakshmi, et al.: *J. Mater. Sci.*, 1984, vol. 19, pp. 2465–72. https://doi.org/10.1007/BF00550799.